ARC Geophysical Research

# Bridging the Gap Between Applied Meteorology and Climate Science: A White Roof Example

Dan Li*[1,2]

[1]Department of Earth and Environment, Boston University, Boston, USA
[2]Department of Mechanical Engineering, Boston University, Boston, USA

**Abstract**

White roof is a widely-studied urban heat mitigation strategy and frequently incorporated into climate adaptation plans by cities. Assessing the effects of white roofs on temperature has often been approached from the perspective of applied meteorology. Here, the white roof problem is reframed as a climate science problem by focusing on the roof surface temperature, incorporating concepts of climate forcing, sensitivity, and feedback, and utilizing a linearized surface energy balance (SEB) model. Different from the Albedo Cooling Effectiveness (ACE) index used for *quantifying* white roof effects, a new index called Albedo Cooling Sensitivity ($\mathrm{ACS_s}$, where the subscript 's' indicates surface) is proposed as a stepping stone towards *understanding* white roof effects. The variability of $\mathrm{ACS_s}$ simulated by the Weather Research and Forecasting (WRF) model is found to be strongly related to the variability of convective heat transfer efficiency. It is recommended that climate forcing, sensitivity, and feedback be systematically integrated into the analysis of diverse urban adaptation strategies.

*Keywords: Urban Heat Mitigation, White Roof, Albedo Cooling Effectiveness, Albedo Cooling Sensitivity*

## 1 Introduction

Urban meteorology and climatology are often viewed as a branch of applied meteorology and climatology [20]. According to [2], applied climatology covers four basic areas: 1) design of structures and planning of activities; 2) assessments of current and past conditions, including

*Corresponding Author
E-mail address: lidan@bu.edu
doi: https://doi.org/10.5149/ARC-GR.1418

evaluation of extreme events; 3) study of the relationships between weather/climate conditions and those in other parts of the physical and socioeconomic worlds; and 4) operation of weather-sensitive systems that employ climatic information in making decisions. Clearly, urban climatology fits into this scope. For example, urban meteorological and climate information is pivotal for the design of buildings and other infrastructure in cities.

As urban populations grow and global temperatures rise, urban meteorology and climatology are playing an increasingly crucial role in fostering more sustainable, resilient, and livable cities. A case in point is climate adaptation, particularly in relation to heat mitigation. One area of active research in urban meteorology and climatology is the assessment of the effectiveness of climate action plans using numerical modeling. This line of research has been primarily approached from the perspective of applied meteorology, where the effects of various adaptation strategies (on temperature and other environmental variables) are quantified for studied cities and periods [e.g. 11].

The premise of this paper is that evaluating the effectiveness of climate action plans offers not only opportunities to test and improve our simulation capabilities, but also new avenues to enhance our understanding of urban climate processes. White roof, a widely studied heat mitigation strategy, is used as an illustrative example.

# 2 Albedo Cooling Effectiveness (ACE)

## 2.1 Definition and Calculation

The basic physics of the white roof problem are straightforward: as the roof surface albedo ($\alpha$) is increased, more solar radiation is reflected and thus less is absorbed, leading to less sensible heating of the near-surface air and less heat conduction into the roof deck and thus building interior. A common theme in urban climate research over the last two decades has been developing physically based modeling tools to simulate the urban environment, based on which the white roof effects can be quantified. A highly successful model for such purposes [3] is the so-called single-layer urban canopy model (SLUCM) [9], where an idealized urban canyon consisting of roof, wall, and canyon floor (Figure 1a) is used to represent three-dimensional, complex urban environments in coarse-resolution weather and climate models (e.g., the Weather Research and Forecasting or WRF model [19]). Using this idealized canyon representation of urban environment, white roofs can be readily simulated by increasing the albedo of the roof facet (c.f., Figure 1c and 1a).

A typical study of SLUCM-enabled simulation of white roof effects is shown in Figure 2. Here the simulations are performed for the greater Boston area over a 5-day heatwave event (July 20-24, 2022, with a spin-up day of July 19) using WRF (version 4.2.2). The domain configurations and physical parameterizations follow a previous study [12], where model validation can be also found. To quantify the white roof effects, two runs are performed: a control run with the roof albedo of 0.2 (Figure 2a) and a high albedo run with the roof albedo of 0.6 (Figure 2b). Here the simulated near-surface air temperature (represented by the widely used 2-m air temperature $T_2$) in the domain with a spatial resolution of 1 km is shown. Focusing on urban grid cells, the majority of urban land experiences lower $T_2$ in the high albedo run (c.f., Figure 2b and 2a), as expected. However, in certain areas $T_2$ increases in the high albedo run (more about this later). The difference between the high albedo run and the control run in terms of $T_2$ (denoted as $\Delta T_2$, where $\Delta$ indicates the difference between the high albedo run and the control run with the high albedo run minus the control run) ranges from -0.6 to 0.2 K (Figure 2c).

An index called Albedo Cooling Effectiveness (ACE) is often used to quantify the effec-

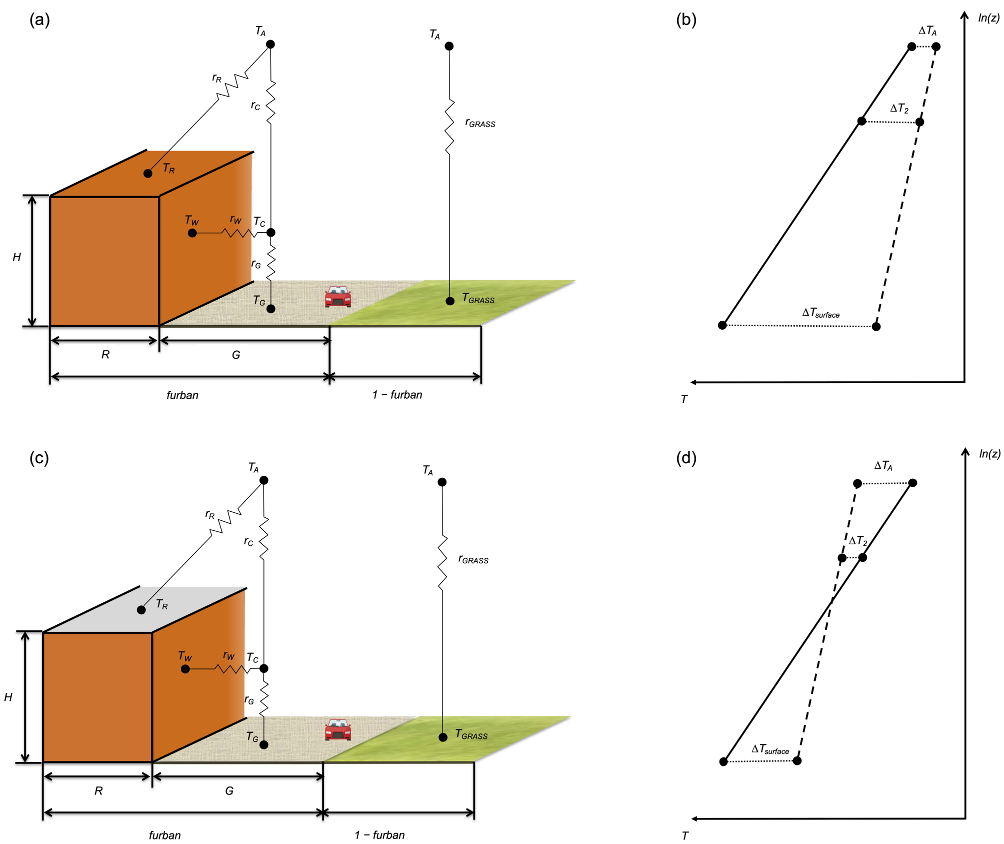


Figure 1: (a) A schematic of the SLUCM in WRF. For each grid cell that is classified as an urban grid cell, WRF-SLUCM treats the grid cell as a combination of an impervious part (with a fraction of $f_{urban}$) and a pervious grass part (with a fraction of $1 - f_{urban}$). In this figure, $T$ is temperature and $r$ is the resistance for heat transfer, and the subscripts A, R, W, C, G, GRASS represent atmosphere, roof, wall, canopy air, canyon ground, and grass, respectively. H, R, G represent the building height, the roof width, and the canyon width, respectively. (c) Similar to (a) but with white roof. (b) A schematic for changes ($\Delta$) in temperatures due to white roofs. The solid line indicates the temperature profile without white roofs and the dashed line indicates the temperature profile with white roofs. White roofs lead to cooler surface temperature $T_{surface}$ of this entire grid cell, which further leads to cooler 2-m air temperature $T_2$ and atmospheric temperature $T_A$. Here it should be emphasized that $T_{surface}$ is an aggregated surface temperature of the entire grid cell, and is not an area-averaged surface temperature across all facets within this grid cell. (d) Similar to (b) except that the atmospheric temperature $T_A$ is increased when white roofs are implemented, leading to increased 2-m air temperature $T_2$. In (b, d), the temperature profile within the surface layer is assumed to be logarithmic for illustration purposes, although in reality the temperature profile is not always logarithmic. A change in the slope of the temperature profile due to white roofs indicates a change of atmospheric stability within the surface layer.

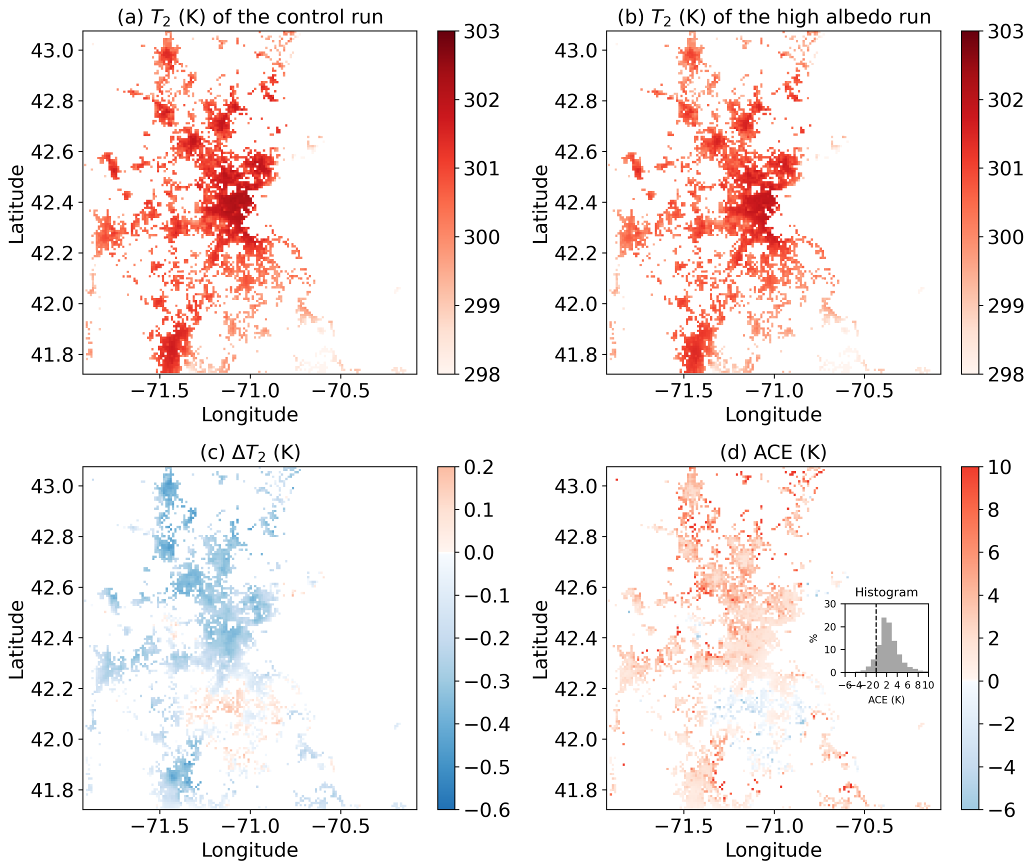


Figure 2: White roof effects on 2-m air temperature ($T_2$) over the greater Boston area simulated by WRF at a spatial resolution of 1 km (roughly corresponding to the neighborhood scale). (a) $T_2$ of the control run (K), (b) $T_2$ of the high albedo run (K), (c) $\Delta T_2$ (K), (d) ACE (K). The inset in (d) shows the histogram of ACE. Only the results over urban grid cells are shown and the results are averaged over a 5-day period from July 20 to July 24, 2022.

tiveness of reflective materials [7, 8], defined as

$$\mathrm{ACE} = -\frac{\Delta T}{\Delta \alpha}, \tag{1}$$

where $\Delta T$ (K) is the change of neighbourhood scale (on the order of a few hundred meters to a kilometer), near-surface air temperature due to the change in the neighbourhood scale albedo ($\Delta\alpha$). The change in the neighbourhood scale albedo ($\Delta\alpha$) can be further expressed as $\Delta\alpha = \Delta\alpha_s f_s$, where the subscript 's' refers to the modified surface. Hence, $\Delta\alpha_s$ is the change in albedo of the modified surface and $f_s$ is the horizontal area of modified surface divided by the horizontal area of the neighborhood. In the WRF results shown in Figure 2d, ACE is computed as $-\Delta T_2/(\Delta\alpha_R f_R)$, where the subscript 'R' indicates that the modified surface is the roof with $\Delta\alpha_R = 0.6 - 0.2 = 0.4$. Note that within each grid cell, only a fraction of land is the impervious land (i.e., $f_{urban}$ in Figure 1a) and only a fraction of the impervious land is roof (i.e., $R/(R+G)$ in Figure 1a). In these WRF simulations, the impervious land fraction varies across the domain, resulting in spatially variable $f_R$.

The ACE values reported by different modeling studies in the literature range from 0 to 20 K, as summarized in a recent review [8]. Focusing on a sub-sample of 47 higher quality modeling studies, the reported ACE values range from 2 to 6 K [8]. In the simulations shown in Figure 2, the majority of ACE values ranges from -2 to 8 K, with a median ACE value of 2.2 K and a mean ACE value of 2.8 K. These median/mean ACE values are within the range reported in previous studies [8].

## 2.2 Transferability and Interpretability

Intercomparing ACE values from different studies may lead to the mistaken perception that ACE is a constant. To be clear, the ACE defined in Eq. 1 *cannot* be constant. At a minimum, it must vary with incoming solar radiation ($SW_{in}$). A simple thought experiment suggests that in regions with stronger solar radiation, the same amount of increase in roof albedo should theoretically result in a greater reduction in air temperature, assuming all other factors remain equal. This is also why seasonally averaged or wintertime ACE values tend to be lower than those during the summer [8].

A complete understanding of the spatio-temporal variability of ACE remains elusive, which poses a problem since, regardless of the indices used to quantify the effects of white roofs, their utility relies on our ability to understand (and even predict) their variability across time and space. Without this understanding, the results reported in the literature would have limited value for reference and, as a result, limited transferability. Under such conditions, the problem becomes strictly an applied one, requiring recalculation of the values of these indices whenever study locations or periods change.

A more subtle issue is that ACE is often defined with near-surface air temperature, which is notoriously difficult to model in urban environments. The 2-m air temperature ($T_2$) from numerical models is widely used to represent the near-surface air temperature. However, its interpretation over complex and tall urban canopies remains a challenge [17]. Even if we assume that $T_2$ is the correct temperature to use in this context, changes in $T_2$ as the roof albedo changes can be difficult to interpret. To demonstrate this, $\Delta T_2$ in Figure 2c is decomposed into contributions from changes in various factors including the roof surface temperature ($T_R$), the atmospheric temperature above the urban canopy ($T_A$), the wall and ground surface temperatures ($T_B$, $T_G$), the grass temperature in the same grid cell ($T_{GRASS}$), and heat transfer resistances (see Figure 1 for the definitions of these temperatures and resistances), following the decomposition method in an earlier study [12].

Here the decomposition is performed separately for grid cells with positive and negative $\Delta T_2$ values to highlight their differences and similarities. It can be seen that for both posi-

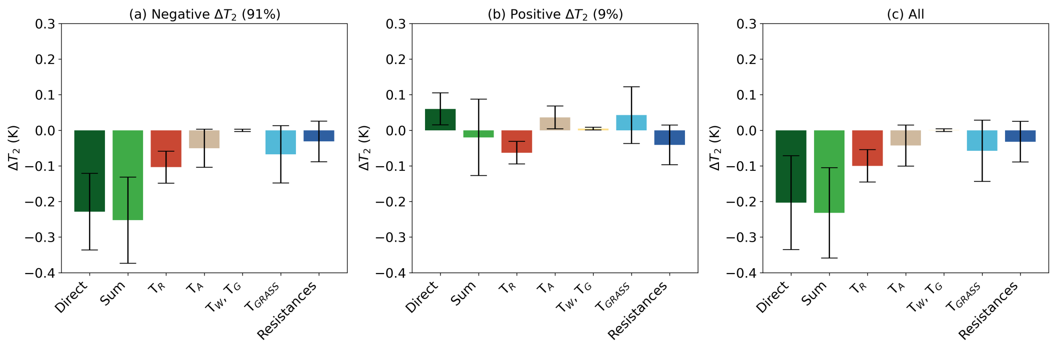


Figure 3: (a) The decomposition of $\Delta T_2$ over urban grid cells with negative $\Delta T_2$ values (91%), (b) The decomposition of $\Delta T_2$ over urban grid cells with positive $\Delta T_2$ values (9%), (c) The decomposition of $\Delta T_2$ over all urban grid cells. The different bars represent, from left to right, computed $\Delta T_2$ directly using WRF outputs, diagnosed $\Delta T_2$ from the decomposition method, contribution from changes in the roof surface temperature ($T_R$), contribution from changes in the atmospheric temperature above the urban canopy ($T_A$), contribution from changes in the wall and ground surface temperatures ($T_W$, $T_G$), contribution from changes in the grass temperature in the same grid cell ($T_{GRASS}$), and contribution from changes in heat transfer resistances. The error bars are standard deviations that indicate spatial variability.

tive and negative $\Delta T_2$ cases, contributions from the roof surface temperature are one of the most important contributions and are consistently negative, implying that the roof surface temperature is always reduced when the roof albedo is increased. This is not surprising given that the cooling signal originates from the roof surface. However, contributions from other factors such as the atmospheric temperature above the urban canopy, the grass temperature, and the heat transfer resistances are not negligible. For negative $\Delta T_2$ cases (Figure 3a), the atmospheric temperature above the urban canopy is also reduced as the roof albedo increases (see Figure 1b for a schematic). However, for positive $\Delta T_2$ cases (Figure 3b), the atmospheric temperature above the urban canopy is increased as the roof albedo increases (see Figure 1d for a schematic). Changes in the atmospheric temperature above the urban canopy are extremely difficult to fully understand especially at the weather time scales, as these changes are strongly affected or even dominated by non-local atmospheric processes. In the simulations shown in Figure 2, it can only be conjectured that in certain regions warm advection causes the atmospheric temperature above the urban canopy ($T_A$) to increase even though the roof surface temperature ($T_R$) is reduced, leading to positive $\Delta T_2$ and thus negative ACE values.

There is no reason why the effects of white roofs cannot be defined using other temperature metrics. In fact, a good candidate is the roof surface temperature ($T_R$), which can serve as an intermediate stepping stone. Intuitively, changes in roof albedo first cause the roof surface temperature to change (see Figure 4a, b), which then drive other changes such as near-surface air temperature, humidity, and wind fields. So the response of roof surface temperature to albedo increase is perhaps *easier* (but not necessarily easy) to understand. This argument is supported by the fact that changes in the roof surface temperature are always negative even in places where changes in $T_2$ are positive, as shown in Figure 4c. For comparison purposes, an $\mathrm{ACE_s}$ (Figure 4d) is defined based on the surface temperature and albedo changes of the modified surface, as follows

$$\mathrm{ACE_s} = -\frac{\Delta T_s}{\Delta \alpha_s}. \tag{2}$$

Again, the subscript 's' refers to the modified surface. In our case, 's' refers to the roof but the definition of $\mathrm{ACE_s}$ is more general and not specific to the roof surface. Here it should

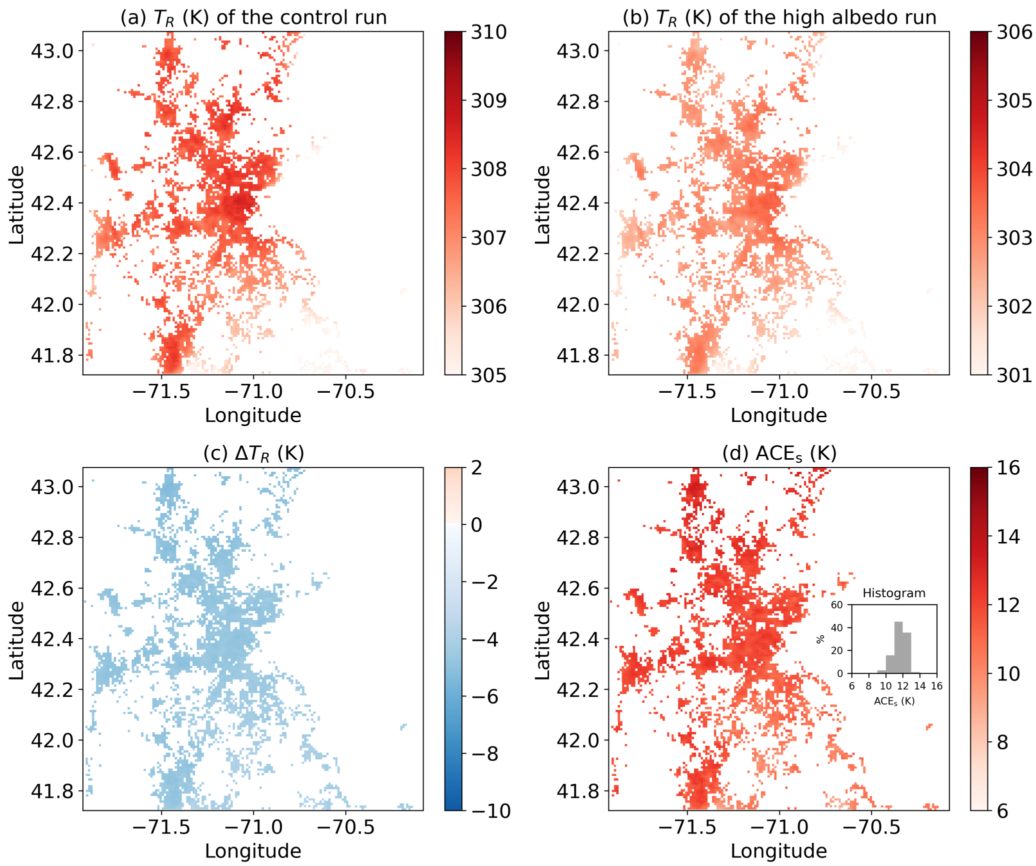


Figure 4: Similar to Figure 2 but for roof surface temperature ($T_R$). (a) $T_R$ of the control run (K), (b) $T_R$ of the high albedo run (K), (c) $\Delta T_R$ (K), (d) $\mathrm{ACE_s}$ (K). The inset in (d) shows the histogram of $\mathrm{ACE_s}$. Only the results over urban grid cells are shown and the results are averaged over a 5-day period from July 20 to July 24, 2022.

also be pointed out that throughout the paper $T_s$, even when defined generally, refers to the surface temperature of a facet (e.g., roof, wall, canyon floor, etc) shown in Figure 1. This is different from $T_{surface}$ in Figure 1(b, d), which refers to an aggregated surface temperature of the entire grid cell. In WRF, $T_{surface}$ is not simply an area-weighted average of the surface temperatures across all urban facets; instead, its calculation is based on an energy balance approach and hence $\Delta T_{surface} \neq \Delta T_s f_s$ [10, 12].

# 3 Albedo Cooling Sensitivity (ACS)

## 3.1 From Cooling Effectiveness to Climate Sensitivity

In climate science, changes in global average temperature ($\Delta T$, K) are often interpreted with the associated climate forcing ($\Delta F$, W m$^{-2}$), which is quantified at the top of the atmosphere and is commonly referred to as the radiative forcing. While quantifying climate forcing at the top of the atmosphere for the white roof problem may be challenging (and unnecessary if we focus on local temperature changes), we can apply a similar concept at the surface. From the surface perspective, the forcing in the white roof problem can be expressed as $SW_{in}(-\Delta\alpha)$, namely, the change of absorbed shortwave radiation assuming that $SW_{in}$ remains constant when the surface albedo is altered. Hence, instead of linking $\Delta T$ to $\Delta\alpha$ as in the ACE

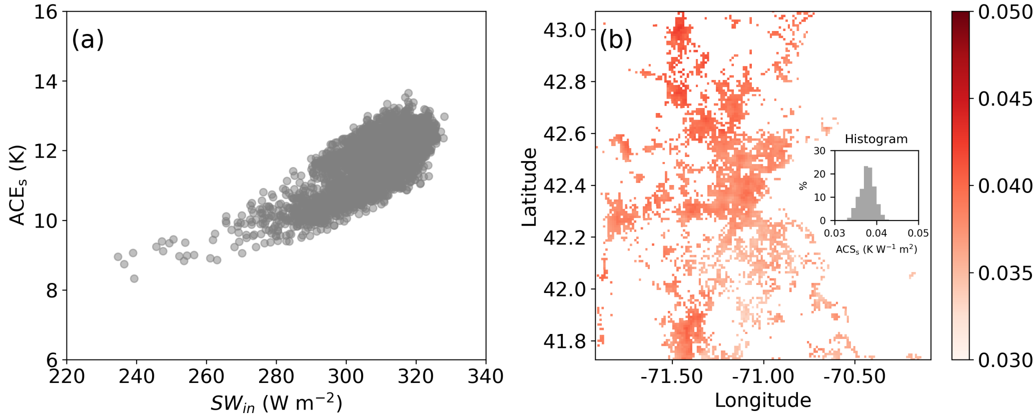


Figure 5: (a) The relation between ACE$_s$ (K) and incoming shortwave radiation ($SW_{in}$, W m$^{-2}$). (b) The spatial pattern of ACS$_s$ (K W$^{-1}$ m$^2$). The inset in (b) shows the histogram of ACS$_s$. Only the results over urban grid cells are shown and the results are averaged over a 5-day period from July 20 to July 24, 2022.

framework, a climate science inspired approach would be linking $\Delta T$ to $SW_{in}(-\Delta\alpha)$.

To differentiate from ACE, this new index will be referred to as the Albedo Cooling Sensitivity (ACS). Given that the forcing used is a surface forcing, ACS probably will work better for understanding surface temperature changes. To emphasize this focus on surface temperature, a subscript 's' is added to $\Delta T$, $\Delta\alpha$ and ACS, as follows:

$$\mathrm{ACS_s} = \frac{\Delta T_s}{SW_{in}(-\Delta\alpha_s)} = -\frac{\Delta T_s}{SW_{in}\Delta\alpha_s} = \frac{\mathrm{ACE_s}}{SW_{in}}. \tag{3}$$

The ACS$_s$ defined this way has a standard unit of K W$^{-1}$ m$^2$ and can be interpreted as a local surface climate sensitivity. Comparing Eq. 3 to Eq. 1, it is clear that ACS$_s$ specifically focuses on surface temperature while ACE focuses on near-surface air temperature. Comparing Eq. 3 to Eq. 2 reveals that ACS$_s$ addresses the $SW_{in}$ dependence of ACE$_s$, as shown in Figure 5a. Not surprisingly, the stronger the $SW_{in}$, the larger the ACE$_s$. However, the scatter in Figure 5a suggests that ACS$_s$ is not a constant, whose spatial pattern is shown in Figure 5b. To understand the spatial variability of ACS$_s$, a linearized surface energy balance (SEB) model [1, 13] is utilized, as discussed below.

### 3.2 A Linearized Surface Energy Balance (SEB) Model for ACS$_s$

For a homogeneous surface (e.g., the roof surface in the SLUCM model), the SEB equation can be written as:

$$SW_{in}(1-\alpha_s) + \varepsilon LW_{in} = H + LE + G + \varepsilon\sigma T_s^4 \tag{4}$$

where $SW_{in}$ and $LW_{in}$ are the incoming shortwave and longwave radiation (W m$^{-2}$), respectively, $\varepsilon$ is the surface emissivity, $H$ is the sensible heat flux (W m$^{-2}$), $LE$ is the latent heat flux (W m$^{-2}$), $G$ is the conductive or ground heat flux (W m$^{-2}$), and $\varepsilon\sigma T_s^4$ is the emitted longwave radiation by the surface (W m$^{-2}$) where $\sigma$ is the Stefan-Boltzmann constant (=5.67×10$^{-8}$ W m$^{-2}$ K$^{-4}$) and $T_s$ is the temperature of the surface (K) to which this SEB equation applies. The emitted longwave radiation is rearranged to the right-hand-side of the surface energy balance equation to emphasize that each term on the right-hand-side of Eq. 4 is a function of $T_s$ while the terms on the left-hand-side of Eq. 4 are assumed to be atmospheric forcing for the surface and are not directly affected by $T_s$.

Each term on the right-hand-side of Eq. 4 is then linearized:

$$H = \lambda_H T_s + C_H, \tag{5}$$

$$LE = \lambda_{LE} T_s + C_{LE} \tag{6}$$

$$G = \lambda_G T_s + C_G, \tag{7}$$

$$\varepsilon \sigma T_s^4 = \lambda_{ELW} T_s + C_{ELW}. \tag{8}$$

Here $\lambda$s and $C$s are the slopes and intercepts of these linear relations, respectively. The $\lambda$s can be viewed as heat transfer efficiencies which have standard units of W m$^{-2}$ K$^{-1}$. The $C$s have standard units of W m$^{-2}$. The full expressions of $\lambda$s and $C$s can be found elsewhere [1, 13] and thus only the key controls of $\lambda$s and $C$s are briefly mentioned here. The convective heat transfer efficiency $\lambda_H$ depends primarily on the wind speed and thermal stratification; the latent heat transfer efficiency $\lambda_{LE}$ also depends on the wind speed and thermal stratification, but more importantly on the moisture and vegetation characteristics of the surface; the conductive heat transfer efficiency $\lambda_G$ is mostly controlled by the heat capacity and thermal conductivity of the ground (or the roof material in our case); the longwave radiative heat transfer efficiency $\lambda_{ELW}$ is only a function of the current air temperature. For the intercepts, $C_H$ depends on the air temperature. Note that in the WRF-SLUCM model, the roof directly interacts with the atmosphere above the canyon. In other words, $H$ is formulated based on the difference between the roof surface temperature and the atmospheric temperature above the canyon ($T_A$, see Figure 1). As a result, $C_H$ depends on $T_A$ in WRF-SLUCM. The intercept $C_{LE}$ depends on the air temperature and air humidity; $C_G$ depends on the deep ground temperature (for the roof in WRF-SLUCM, $C_G$ depends on the building interior temperature); $C_{ELW}$ is only a function of the current air temperature. For completely dry and non-evaporating roofs, $\lambda_{LE} = 0$ and $C_{LE} = 0$.

With this linear assumption, the SEB can be interpreted using Figure 6, where the horizontal black solid line represents the left-hand-side of Eq. 4 and is independent of $T_s$ while the red line represents the right-hand-side Eq. 4 and is a linear function of $T_s$ with a slope of $\lambda_H + \lambda_{LE} + \lambda_G + \lambda_{ELW}$. The intersection of these two lines indicates an energy balance state. When the surface albedo is increased by $\Delta\alpha_s$, the left-hand-side of Eq. 4 is reduced by $SW_{in}(-\Delta\alpha_s)$, assuming that $SW_{in}$ and $\varepsilon LW_{in}$ remain constant. On Figure 6, it means that the horizontal black solid line is moved downward by $SW_{in}(-\Delta\alpha_s)$ (i.e., it becomes the horizontal black dashed line). Further assuming that the red line stays where it is, the change in the surface temperature can be readily obtained from simple geometry on Figure 6, as follows:

$$\Delta T_s = \frac{SW_{in}(-\Delta\alpha_s)}{\lambda_H + \lambda_{LE} + \lambda_G + \lambda_{ELW}}, \tag{9}$$

which gives

$$\mathrm{ACS_s} = \frac{\Delta T_s}{SW_{in}(-\Delta\alpha_s)} = \frac{1}{\lambda_H + \lambda_{LE} + \lambda_G + \lambda_{ELW}}. \tag{10}$$

The beauty of $\mathrm{ACS_s}$, as now demonstrated in Eq. 10, is that it can be related to various heat transfer efficiencies. These heat transfer efficiencies are equivalent to climate feedback parameters widely used in the climate science literature. Therefore, one might argue that by introducing the $\mathrm{ACS_s}$ index and utilizing the linearized SEB model, the white roof problem, which has long been approached from the perspective of applied meteorology, is now reframed as a climate science problem. Eq. 10 clearly shows that $\mathrm{ACS_s}$ cannot be a constant as the

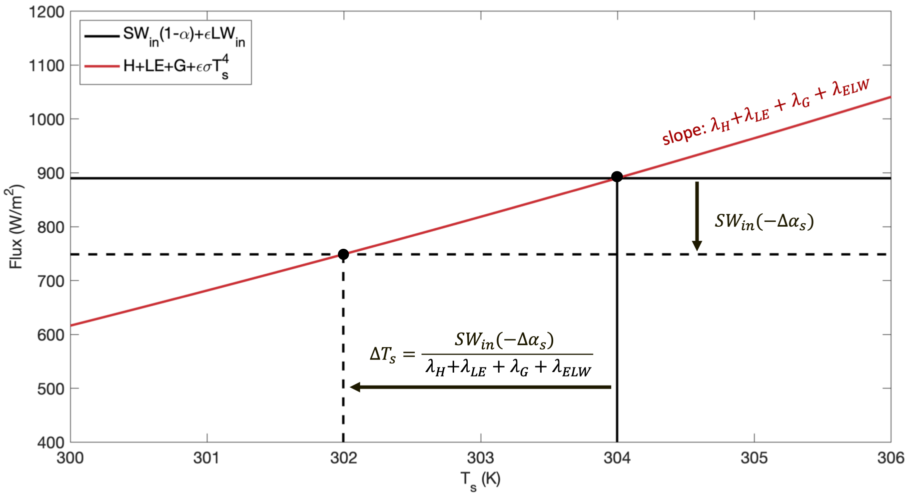


Figure 6: A linearized SEB model for $\mathrm{ACS}_s$. The black solid line (horizontal) represents the left-hand-side of Eq. 4 and is independent of $T_s$ while the red line represents the right-hand-side Eq. 4 and is a linear function of $T_s$ with a slope of $\lambda_H + \lambda_{LE} + \lambda_G + \lambda_{ELW}$. The intersection of these two lines indicates an energy balance state. The black dashed line (horizontal) represents the left-hand-side of Eq. 4 when the albedo is increased by $\Delta\alpha_s$.

heat transfer efficiencies or climate feedback parameters vary with meteorological and surface conditions [1, 13].

Eq. 10 is the simplest case where the four feedbacks are the most fundamental, stabilizing feedbacks in the studied system (in this case, the surface). By analogy, they are similar to the Planck feedback (also referred to as the Planck response) in the context of global climate change. One can incorporate additional feedback parameters. To do so, the right-hand-side of the SEB equation (Eq. 4) is first denoted as $R$, namely, $R = H + LE + G + \varepsilon\sigma T_s^4$. The difference caused by an increase in the roof albedo on both sides of the SEB equation still has to be balanced, namely, $\Delta\left[SW_{in}(1-\alpha_s) + \varepsilon LW_{in}\right] = \Delta R$. Further assuming that $SW_{in}$ and $\varepsilon LW_{in}$ are not affected by the increase in roof albedo results in $SW_{in}(-\Delta\alpha_s) = \Delta R$. Hence, the $\mathrm{ACS_s}$ can be expressed as

$$\mathrm{ACS_s} = \frac{\Delta T_s}{SW_{in}(-\Delta\alpha_s)} = \frac{\Delta T_s}{\Delta R} = \frac{1}{\frac{\Delta R}{\Delta T_s}}. \tag{11}$$

Since $R = H + LE + G + \varepsilon\sigma T_s^4 = (\lambda_H + \lambda_{LE} + \lambda_G + \lambda_{ELW})T_s + (C_H + C_{LE} + C_G + C_{ELW})$, we can further derive

$$\begin{aligned}\frac{\Delta R}{\Delta T_s} &= \frac{\partial R}{\partial T_s} \\ &+ \frac{\partial R}{\partial \lambda_H}\frac{\Delta\lambda_H}{\Delta T_s} + \frac{\partial R}{\partial \lambda_{LE}}\frac{\Delta\lambda_{LE}}{\Delta T_s} + \frac{\partial R}{\partial \lambda_G}\frac{\Delta\lambda_G}{\Delta T_s} + \frac{\partial R}{\partial \lambda_{ELW}}\frac{\Delta\lambda_{ELW}}{\Delta T_s} \\ &+ \frac{\partial R}{\partial C_H}\frac{\Delta C_H}{\Delta T_s} + \frac{\partial R}{\partial C_{LE}}\frac{\Delta C_{LE}}{\Delta T_s} + \frac{\partial R}{\partial C_G}\frac{\Delta C_G}{\Delta T_s} + \frac{\partial R}{\partial C_{ELW}}\frac{\Delta C_{ELW}}{\Delta T_s},\end{aligned} \tag{12}$$

where

$$\frac{\partial R}{\partial T_s} = \lambda_H + \lambda_{LE} + \lambda_G + \lambda_{ELW}. \tag{13}$$

Substituting Eqs. 12 and 13 into Eq. 11 yields a full equation for $\mathrm{ACS_s}$, as follows:

$$\mathrm{ACS_s} = \frac{1}{\begin{array}{c}\lambda_H + \lambda_{LE} + \lambda_G + \lambda_{ELW} + \\ \frac{\partial R}{\partial \lambda_H}\frac{\Delta\lambda_H}{\Delta T_s} + \frac{\partial R}{\partial \lambda_{LE}}\frac{\Delta\lambda_{LE}}{\Delta T_s} + \frac{\partial R}{\partial \lambda_G}\frac{\Delta\lambda_G}{\Delta T_s} + \frac{\partial R}{\partial \lambda_{ELW}}\frac{\Delta\lambda_{ELW}}{\Delta T_s} + \\ \frac{\partial R}{\partial C_H}\frac{\Delta C_H}{\Delta T_s} + \frac{\partial R}{\partial C_{LE}}\frac{\Delta C_{LE}}{\Delta T_s} + \frac{\partial R}{\partial C_G}\frac{\Delta C_G}{\Delta T_s} + \frac{\partial R}{\partial C_{ELW}}\frac{\Delta C_{ELW}}{\Delta T_s}\end{array}}. \tag{14}$$

It is now clear that Eq. 10 is a simplified version of Eq. 14 by assuming $\Delta R/\Delta T_s \approx \partial R/\partial T_s$ (or equivalently, by assuming the red line on Figure 6 remains unchanged when the surface albedo is altered). This assumption is not always valid. For example, $\lambda_H$ might change when the surface albedo is altered, as atmospheric stability increases and convective heat transfer becomes less efficient with a higher surface albedo due to reduced sensible heat flux. This change of $\lambda_H$ alters the slope of the red line on Figure 6. The significance of such feedback can be quantified by the term $\frac{\partial R}{\partial \lambda_H}\frac{\Delta\lambda_H}{\Delta T_s}$, which can be viewed as a new feedback parameter. However, fully understanding the importance of these new feedback parameters is outside the scope of this study.

Before applying Eq. 10 to analyzing the WRF simulation results, it is important to comment on the relevant time scales. Eq. 10 relies on the linear relations between four fluxes and surface temperature (Eqs. 5-8) and ignores many feedbacks such as the change of $\lambda_H$. These assumptions tend to work better at long-term time scales (e.g., averages over all summer months within a 30-year period). At long-term time scales, Eq. 10 can be used to interpret the spatial variability [22] and other variability (e.g., introduced by varying model parameterizations) of white roof effects. At short time scales, Eq. 10 has to be used carefully or should not be used. For example, Eq. 10 cannot be used to interpret the nighttime effects of white roofs, since treating $SW_{in}(-\Delta\alpha)$ as the forcing is problematic at night when the incoming shortwave radiation is zero. This is partly why the WRF results presented earlier have been averaged over the entire simulation period, without separating daytime from nighttime. However, the time scale remains short since the WRF simulations only span five days. Whether Eq. 10 can be used to interpret the spatial variability of white roof effects at multi-day time scales remains unclear, which frames the scope of the following section. Here it's noted that multi-day simulations are commonly used to assess white roof effects in the urban climate literature [e.g. 11, 14, 18, 26] and thus addressing the applicability of Eq. 10 at multi-day time scales has practical value.

### 3.3 The Variability of $\mathrm{ACS_s}$ and the Role of Convective Heat Transfer Efficiency

As alluded to earlier, in this section Eq. 10 is used to interpret the spatial variability of $\mathrm{ACS_s}$ simulated by WRF, as shown in Figure 5b. This spatial variability represents the neighborhood-to-neighborhood variability, not the city-to-city variability. Moreover, two sensitivity cases are conducted where different planetary boundary layer (including surface layer) parameterizations are used. The planetary boundary layer (including surface layer) parameterizations represent the effects of turbulence and turbulent transport in the atmosphere, which can strongly modulate the dynamics of surface temperature and near-surface air temperature. Specifically, the default case (results already presented earlier) uses the YSU scheme [4, 5], and the two sensitivity cases use the MYNN [15, 16] and MYJ [6, 15] schemes, respectively. These sensitivity tests are not meant to be exhaustive, but rather to demonstrate the utility of Eq. 10.

Figure 7(a, b, c) show the probability density functions (PDFs) of ACE (defined again based on $T_2$), $\mathrm{ACE_s}$, and $\mathrm{ACS_s}$, respectively. The PDFs are estimated using Kernel density estimation, a non-parametric method that smooths discrete data points into a continuous distribution. It is clear that all three indices vary spatially within each case and vary across cases. The ACE values range from -5 to 10 K, the $\mathrm{ACE_s}$ values vary between 8 and 14 K, while the $\mathrm{ACS_s}$ values range between 0.03 and 0.045 K $\mathrm{W^{-1}\ m^2}$. Interestingly, when the YSU scheme is replaced by the MYNN and MYJ schemes, the negative ACE values become much less. These results indicate that the simulated white roof effects are sensitive to turbulence parameterizations.

While the values of $\mathrm{ACS_s}$ cannot be directly compared to those of $\mathrm{ACE_s}$ and ACE due to differences in their dimensions, we can use the coefficients of variation, which are dimensionless, to characterize their variability. For each case where the variability is due to spatial variations, the coefficients of variation for $\mathrm{ACS_s}$ and $\mathrm{ACE_s}$ are of the same order of magnitude, but are an order of magnitude smaller than those for ACE. Comparing $\mathrm{ACS_s}$ to $\mathrm{ACE_s}$, the coefficients of variation are always smaller for $\mathrm{ACS_s}$; namely, the variability of $\mathrm{ACS_s}$ is more constrained than that of $\mathrm{ACE_s}$. This result implies that part of the spatial variability associated with $\mathrm{ACE_s}$ is caused by the spatial variability of $SW_{in}$, as can be inferred from Figure 5a.

When compared across different cases, the MYNN case has very different $\mathrm{ACE_s}$ values compared to the YSU case, but their $\mathrm{ACS_s}$ values are similar. This is due to the fact that $SW_{in}$ are different between these two cases (Figure 8a). Therefore, normalizing $-\Delta T_s/\Delta\alpha_s$ by $SW_{in}$ (i.e., moving from $\mathrm{ACE_s}$ to $\mathrm{ACS_s}$) helps reduce the variability caused by $SW_{in}$ across cases. Note that the variability of $SW_{in}$ caused by changing turbulence parameterizations is quite small (on the order of 20-40 W $\mathrm{m^{-2}}$, as can be seen from Figure 8a). Even for such small variability of $SW_{in}$, it is still better to approach the roof surface temperature change from the perspective of $\mathrm{ACS_s}$ rather than $\mathrm{ACE_s}$. For large variability of $SW_{in}$ (e.g., when studying city-to-city variability or seasonal variability of white roof effects), normalizing $-\Delta T_s/\Delta\alpha_s$ by $SW_{in}$ will be more important as shall be seen later.

MYJ and YSU cases have similar $SW_{in}$ (Figure 8a), yet their $\mathrm{ACS_s}$ values differ strongly (Figure 7c), suggesting that other factors must influence the results. Close inspection reveals that the MYJ case has a smaller near-surface wind speed than the YSU case (Figure 8b). The linearized SEB model provides the necessary tools to understand why $\mathrm{ACS_s}$ is increased with reduced near-surface wind speed. As shown in Figure 7d, $\mathrm{ACS_s}$ is a strong function of $\lambda_H$, the convective heat transfer efficiency. In neighborhoods with weaker convective heat transfer efficiency caused by reduced near-surface wind speed, the $\mathrm{ACS_s}$ values are larger (c.f. MYJ to YSU in Figure 7c, d). Physically, this occurs because with weaker convective heat transfer efficiency, the roof surface temperature tends to be much higher, as less heat is transferred into the atmosphere. Under such conditions, increasing the roof albedo results in a more pronounced reduction in roof surface temperature. Conversely, when heat is efficiently convected into the atmosphere and the roof surface temperature is already low, increasing the roof albedo has a smaller impact.

However, the objective here is not to determine why different planetary boundary layer parameterizations yield varying $SW_{in}$ and wind speed. Instead, the focus is on interpreting the simulated $\mathrm{ACS_s}$ using the linearized SEB model (Eq. 10). For each case, the spatial variability of $\lambda_H$ is found to be a key control of the spatial variability of $\mathrm{ACS_s}$, as shown in Figure 7d. To fully grasp this point, we need to take a closer look at the four climate feedback parameters in these WRF simulations. As discussed, $\lambda_H$ is the convective heat transfer efficiency and thus depends on the wind speed and thermal stratification. Hence, $\lambda_H$ is expected to vary spatially (and with turbulence parameterizations). In these simulations, $\lambda_H$ varies between 12 to 22 W $\mathrm{m^{-2}\ K^{-1}}$, as shown in Figure 7d. On the other hand, $\lambda_{LE}$, $\lambda_G$, and $\lambda_{ELW}$ have limited spatial variability in these simulations. During the simulation period, there is no rainfall and the roof is completely dry, leading to $\lambda_{LE} = 0$. The $\lambda_G$ is largely determined by roof thermal properties (especially heat capacity and thermal conductivity)[13], which are prescribed inputs

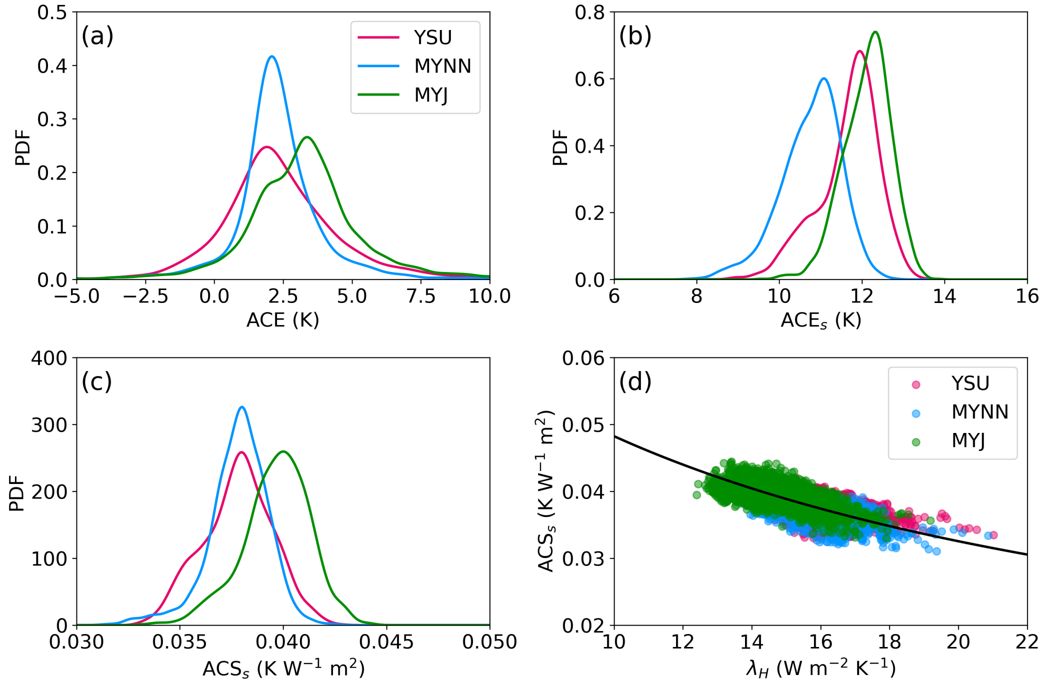


Figure 7: PDFs of (a) ACE, (b) ACE$_s$, (c) ACS$_s$; (d) the relation between ACS$_s$ and $\lambda_H$ where the black line is a fitted curve based on Eq. 10, given by ACS$_s = 1/(\lambda_H + 10.73)$. Only the results over urban grid cells are included and the results are averaged over a 5-day period from July 20 to July 24, 2022.

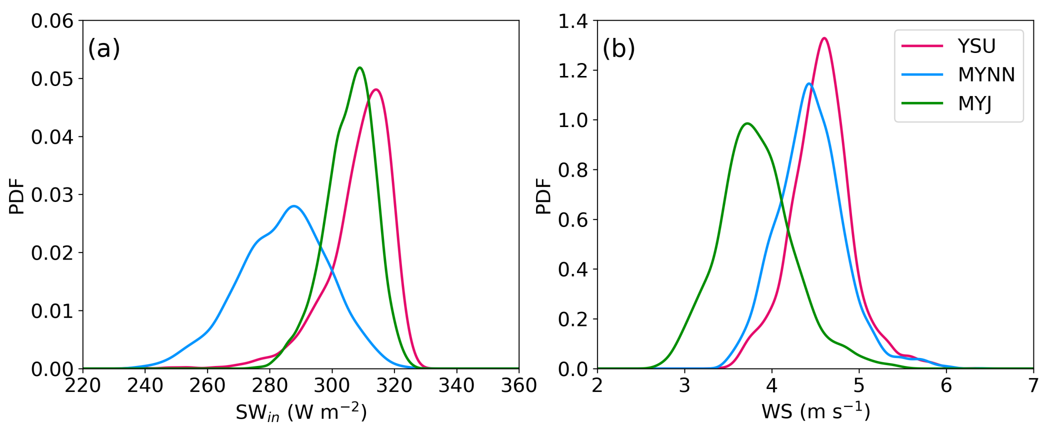


Figure 8: PDFs of (a) $SW_{in}$ and (b) 10-m wind speed ($WS$) in the control runs (i.e., the roof albedo of 0.2). Only the results over urban grid cells are included and the results are averaged over a 5-day period from July 20 to July 24, 2022.

and do not vary across the domain [12]. The $\lambda_{ELW}$ scales with $T_A^3$ and thus does not vary strongly in space given that $T_A$ is generally on the order of 300 K, yielding $\lambda_{ELW} \approx 6$ W m$^{-2}$ K$^{-1}$. The function $\mathrm{ACS_s} = 1/(\lambda_H + C)$ (the black line in Figure 7d) provides a good fit to the simulation results, where $C$ is determined via nonlinear least squares regression as 10.73 $\pm$ 0.02. The fitted $C$ value (unit: W m$^{-2}$ K$^{-1}$) and that $\lambda_{ELW} \approx 6$ W m$^{-2}$ K$^{-1}$ suggest that $\lambda_G \approx 4.7$ W m$^{-2}$ K$^{-1}$. This is consistent with previous work suggesting that $\lambda_G$ has similar magnitude as $\lambda_{ELW}$ but is much smaller than $\lambda_H$ [1]. In summary, only $\lambda_H$ exhibits strong spatial variability in these simulations, while the spatial variability of the other three feedback parameters is limited, explaining why the spatial variability of $\lambda_H$ is a key control of the spatial variability of ACS$_\mathrm{s}$. This does not mean that the spatial variability of these other feedback parameters is always not important. Since they are dependent on meteorological conditions and urban hygrothermal properties, their spatial variability may become relevant under certain circumstances [22].

To corroborate these findings, similar simulations are conducted for a wintertime period (Feb 10-14, 2022, with a spin-up day of Feb 9) when the average incoming solar radiation is about 100 W m$^{-2}$ (i.e., about 1/3 of the average incoming solar radiation during the summertime period). The analysis is repeated and results are shown in Figure 9. Comparing Figure 9 to Figure 7 reveals that the ACE and ACE$_\mathrm{s}$ values differ strongly between summer and winter periods. In contrast, the ACS$_\mathrm{s}$ values are more consistent between the two periods. Among the three indices, the coefficients of variation are the smallest for ACS$_\mathrm{s}$, again highlighting the importance of normalization by $SW_{in}$. Moreover, the variability of ACS$_\mathrm{s}$ is largely explained by $\lambda_H$ (e.g., the MYJ case again has the largest ACS$_\mathrm{s}$ values because of the smallest near-surface wind speeds). However, the fitted line in Figure 9d becomes $\mathrm{ACS_s} = 1/(\lambda_H + 7.31)$. The value of 7.31 $\pm$ 0.01 (unit: W m$^{-2}$ K$^{-1}$) is reduced compared to its summer counterpart, partly due to the reduction of $\lambda_{ELW}$ to about 4.5 W m$^{-2}$ K$^{-1}$ at 270 K.

These results demonstrate the utility of the linearized SEB framework. While not all feedback parameters are readily available or can be easily computed such as $\lambda_G$ at short time scales, the physical insights offered by the linearized SEB framework underscore its value as a *diagnostic* tool for understanding the variability of ACS$_\mathrm{s}$.

# 4 Final Remarks

By focusing on the roof surface temperature and utilizing concepts like climate forcing, sensitivity, and feedback, the white roof problem is reframed as a climate science problem. A new index called Albedo Cooling Sensitivity (ACS$_\mathrm{s}$) is proposed and a linearized SEB model is utlized to understand the variability of ACS$_\mathrm{s}$. The spatial variability of ACS$_\mathrm{s}$ simulated by WRF and the influence of turbulence parameterizations on ACS$_\mathrm{s}$ are examined, where the convective heat transfer efficiency is found to play an important role.

The purpose of this paper is not to discredit the concept of ACE, but rather to provide a stepping stone towards understanding the white roof effects. The ACS$_\mathrm{s}$ concept could and perhaps should be used jointly with ACE. More broadly, approaching urban adaptation challenges from the perspective of climate science can generate new insights that could not be obtained if these problems were only treated in the realm of applied meteorology. The use of concepts of forcing, sensitivity, and feedback should be embraced. A few more research examples are briefly discussed to emphasize the value of these concepts. First, [23] examined the cooling benefits of irrigation on green roofs and treated the change of latent heat flux due to irrigation as the forcing (unlike in the model presented here where the change of latent heat flux is viewed as a response). Their model successfully explained the spatial variability of cooling benefits of green roof irrigation. Second, previous studies found that urban trees' cooling efficiency, defined as the magnitude of land surface temperature reduction per 1%

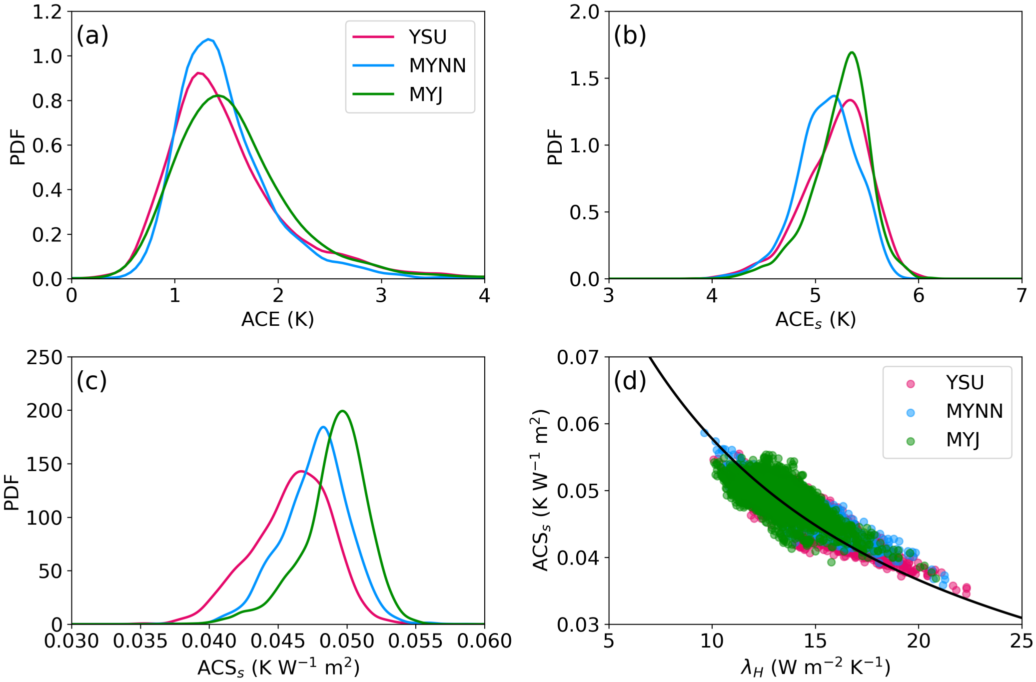


Figure 9: PDFs of (a) ACE, (b) ACE$_\mathrm{s}$, (c) ACS$_\mathrm{s}$; (d) the relation between ACS$_\mathrm{s}$ and $\lambda_H$ where the black line is a fitted curve based on Eq. 10, given by ACS$_\mathrm{s} = 1/(\lambda_H + 7.31)$. Only the results over urban grid cells are included and the results are averaged over a 5-day period from Feb 10 to Feb 14, 2022.

increase in fractional tree cover, tends to be stronger in hot and dry cities [25]. This can be understood again from the perspective of changes in the latent heat flux (the forcing): a 1% increase in fractional tree cover tends to result in a stronger increase in latent heat flux in hot and dry regions than in cool and humid regions where latent heat flux is more controlled by energy availability. Third, [24] reviewed previous modeling studies on the warming effects of anthropogenic heat flux ($Q_{AH}$) and found large discrepancies in terms of changes of urban air temperature ($\Delta T$) due to anthropogenic heat fluxes. However, the sensitivity of urban air temperature to anthropogenic heat flux ($\Delta T/\Delta Q_{AH}$) showed consistency across studies. They further found that feedbacks introduced by convective heat transfer efficiency and its variation were key to explaining the seasonal variations of $\Delta T/\Delta Q_{AH}$. These research examples further demonstrate the power of concepts of climate forcing, sensitivity, and feedback in urban adaptation research.

Lastly, can concepts of climate forcing, sensitivity, and feedback still offer insights if the focus was near-surface air temperature? This remains an open question. First, even for the white roof problem it is unclear whether $SW_{in}(-\Delta\alpha)$ represents a forcing for the near-surface air, as it does not enter the energy budget of near-surface air. Perhaps a better candidate is $\Delta H$, which is still related to $SW_{in}(-\Delta\alpha)$ especially at long-term time scales. Second, unlike the one-dimensional SEB equation which provides a framework for understanding surface temperature dynamics, the energy budget of near-surface air is three-dimensional (unless some idealization is applied to the near-surface air such as the urban canopy air in SLUCMs [24] or the constant flux layer [21]) and thus much more complicated. It is unclear whether the near-surface air budget can provide the same general framework like the SEB equation based on which sensitivities and feedback parameters can be connected. Addressing these challenges are left for future work.

## Acknowledgements

This research was supported by the U.S. Department of Energy, Office of Science, as part of research in MultiSector Dynamics, Earth and Environmental System Modeling Program. The work used resources of the National Energy Research Scientific Computing Center (NERSC), a U.S. Department of Energy Office of Science User Facility located at Lawrence Berkeley National Laboratory, operated under Contract No. DE-AC02- 05CH11231, as well as the high-performance computing support from Derecho (https://doi.org/ 10.5065/qx9a-pg09) provided by NCAR's Computational and Information Systems Laboratory, sponsored by the National Science Foundation. This research was also supported by an unrestricted gift from Google, but the statements, findings, and conclusions do not necessarily reflect the views of Google. Finally, I would like to thank Mingze Ding, Xiaojing Tang, and Ting Sun for reviewing earlier versions of this essay, and Lucy Hutyra, David Fork, Jiachuan Yang, and Ning Zhang for valuable discussions. The comments from two anonymous reviewers are also acknowledged.


## Data Availability

The WRF outputs of this work were produced with a modified version of WRF v4.2.2, which can be found at https://doi.org/10.5281/zenodo.14611848. The scripts to reproduce the figures are documented at https://github.com/IMMM-SFA/li_2025_ARC/tree/main.

## Author Contributions

**DL:** Conceptualization; Data Curation; Formal Analysis; Funding Acquisition; Methodology; Software; Visualization; Writing – Original Draft Preparation; Writing – Review & Editing.

## References


[1] S. Bateni and D. Entekhabi. Relative efficiency of land surface energy balance components. *Water Resources Research*, 48(4), 2012.

[2] S. A. Changnon. Applied climatology: The golden age has begun. *Bulletin of the American Meteorological Society*, 86(7):915–919, 2005.

[3] J. Garratt, J. Wilczak, A. Holtslag, H. P. Schmid, A. Grachev, A. Beljaars, T. Foken, F. Chen, C. Fairall, B. Hicks, et al. Commentaries on top-cited boundary-layer meteorology articles. *Boundary-Layer Meteorology*, 177:169–188, 2020.

[4] S.-Y. Hong. A new stable boundary-layer mixing scheme and its impact on the simulated East Asian summer monsoon. *Quarterly Journal of the Royal Meteorological Society*, 136 (651):1481–1496, 2010.

[5] S.-Y. Hong, Y. Noh, and J. Dudhia. A new vertical diffusion package with an explicit treatment of entrainment processes. *Monthly weather review*, 134(9):2318–2341, 2006.

[6] Z. Janjic. Nonsingular implementation of the Mellor-Yamada Level 2.5 Scheme in the NCEP Meso model, National Centers for Environmental Prediction. *Office Note# 437*, pages 1–61, 2001.

[7] E. S. Krayenhoff and J. A. Voogt. Impacts of urban albedo increase on local air temperature at daily–annual time scales: Model results and synthesis of previous work. *Journal of Applied Meteorology and Climatology*, 49(8):1634–1648, 2010.

[8] E. S. Krayenhoff, A. M. Broadbent, L. Zhao, M. Georgescu, A. Middel, J. A. Voogt, A. Martilli, D. J. Sailor, and E. Erell. Cooling hot cities: a systematic and critical review of the numerical modelling literature. *Environmental Research Letters*, 16(5):053007, 2021.

[9] H. Kusaka, H. Kondo, Y. Kikegawa, and F. Kimura. A simple single-layer urban canopy model for atmospheric models: Comparison with multi-layer and slab models. *Boundary-layer meteorology*, 101:329–358, 2001.

[10] D. Li and E. Bou-Zeid. Quality and sensitivity of high-resolution numerical simulation of urban heat islands. *Environmental Research Letters*, 9(5):055001, 2014.

[11] D. Li, E. Bou-Zeid, and M. Oppenheimer. The effectiveness of cool and green roofs as urban heat island mitigation strategies. *Environmental Research Letters*, 9(5):055002, 2014.

[12] D. Li, T. Sun, J. Yang, N. Zhang, P. Vahmani, and A. Jones. Structural uncertainty in the sensitivity of urban temperatures to anthropogenic heat flux. *Journal of Advances in Modeling Earth Systems*, 16(10):e2024MS004431, 2024.

[13] D. Li, L. Wang, W. Liao, T. Sun, G. Katul, E. Bou-Zeid, and B. Maronga. Persistent urban heat. *Science Advances*, 10(15):eadj7398, 2024.

[14] X.-X. Li and L. K. Norford. Evaluation of cool roof and vegetations in mitigating urban heat island in a tropical city, Singapore. *Urban Climate*, 16:59–74, 2016.

[15] G. L. Mellor and T. Yamada. Development of a turbulence closure model for geophysical fluid problems. *Reviews of Geophysics*, 20(4):851–875, 1982.

[16] M. Nakanishi and H. Niino. Development of an improved turbulence closure model for the atmospheric boundary layer. *Journal of the Meteorological Society of Japan. Ser. II*, 87(5):895–912, 2009.

[17] Y. Qin, W. Liao, and D. Li. Attributing the urban–rural contrast of heat stress simulated by a global model. *Journal of Climate*, 36(6):1805–1822, 2023.

[18] A. Sharma, P. Conry, H. Fernando, A. F. Hamlet, J. Hellmann, and F. Chen. Green and cool roofs to mitigate urban heat island effects in the Chicago metropolitan area: Evaluation with a regional climate model. *Environmental Research Letters*, 11(6):064004, 2016.

[19] W. C. Skamarock, J. B. Klemp, J. Dudhia, D. O. Gill, Z. Liu, J. Berner, W. Wang, J. Powers, M. Duda, D. Barker, et al. A description of the advanced research WRF version 4. *NCAR tech. note ncar/tn-556+ str*, 145, 2019.

[20] C. Souch and S. Grimmond. Applied climatology: urban climate. *Progress in physical geography*, 30(2):270–279, 2006.

[21] L. Wang and D. Li. Urban heat islands during heat waves: A comparative study between Boston and Phoenix. *Journal of Applied Meteorology and Climatology*, 60(5):621–641, 2021.

[22] L. Wang, M. Huang, and D. Li. Where are white roofs more effective in cooling the surface? *Geophysical Research Letters*, 47(15):e2020GL087853, 2020.

[23] L. Wang, M. Huang, and D. Li. Strong influence of convective heat transfer efficiency on the cooling benefits of green roof irrigation. *Environmental Research Letters*, 16(8): 084062, 2021.

[24] L. Wang, T. Sun, W. Zhou, M. Liu, and D. Li. Deciphering the sensitivity of urban canopy air temperature to anthropogenic heat flux with a forcing-feedback framework. *Environmental Research Letters*, 18(9):094005, 2023.

[25] Q. Yang, X. Huang, X. Tong, C. Xiao, J. Yang, Y. Liu, and Y. Cao. Global assessment of urban trees' cooling efficiency based on satellite observations. *Environmental Research Letters*, 17(3):034029, 2022.

[26] T. Zhong, N. Zhang, and M. Lv. A numerical study of the urban green roof and cool roof strategies' effects on boundary layer meteorology and ozone air quality in a megacity. *Atmospheric Environment*, 264:118702, 2021.